JOURNAL OF COMPUTATIONAL PHYSICS 111, 336–346 (1994)

Boundary Surface Dynamics: An Algorithm for Stratified Geostrophic Flows

FERNANDO VIERA

The School of Mathematics and Statistics, The University of Sydney, NSW, 2006, Australia

Received March 4, 1993; revised October 18, 1993

Assuming three-dimensional stratified geostrophic vortices of finite volume and potential vorticity of arbitrary vertical structure but piecewise-constant distribution in the horizontal direction, we derive equations for the velocity field in terms of surface integrals over the boundary of the vortex regions. Using conservation of quasi-geostrophic potential vorticity and the concepts of contour dynamics, the three-dimensional problem is reduced to the Lagrangian evolution of the boundary surface enclosing the vortex region, thus decreasing the number of dimensions by one. The equations are discretized in space and time giving a simple and robust algorithm for the evolution of the flow with specified initial conditions. The model is used to study the interaction of two identical cylindrical vortices of finite height in a spatially unbounded fluid. For vortices at the same level the simulations show that if the horizontal scale is larger than the internal radius of deformation, filamentation is virtually suppressed and the resulting structure is a compact cylindrical vortex of *ellipse-like* cross section. For vortices at different levels the interaction results in a structure of considerable horizontal and vertical complexity due to the combined effects of merger and alignment processes acting together.

1. INTRODUCTION

Investigations of high Reynolds number turbulent flows in both, two-dimensional Eulerian and geostrophic fluids, have demonstrated the important role played by isolated, coherent structures. In particular, the studies in [4, 5] have revealed the emergence of coherent vortices from random initial conditions in stratified geostrophic turbulence. It appears that a detailed study of their behaviour is essential for a deeper understanding of turbulent flows. As pointed out by *Rhines* [10], it is unlikely that a strongly turbulent fluid can be understood until the nature of its energy-containing eddies is rationalized.

On the theoretical side, the method of contour dynamics [11] has proved to be a powerful technique for the numerical simulation of coherent vortices in two-dimensional inviscid flows. If the vorticity consists of piecewise-constant finite-area vortex regions, the two-dimensional problem can be reduced to the evolution of the one-dimensional closed curve enclosing the area of the vortex region, thus reducing the dimensionality by one. The method has also been applied to the study of quasi-geostrophic vortices using two-layer models [3, 7, 8]. These studies highlight the importance of the effects of stratification and vertical structure on the evolution of coherent vortices and their relationship to the baroclinic-to-barotropic energy cascade in geostrophic turbulence (see, for example, the alignment process studied in [8]).

Motivated by the success of the aformentioned studies, in this article we apply the concepts of contour dynamics to develop boundary surface dynamics (BSD), a numerical algorithm for fully three-dimensional (3D) continuously stratified quasi-geostrophic flows. BSD has all the advantages of contour dynamics, among which is the well-known property of Lagrangian methods to simulate high resolution complex flows at high Reynolds numbers characterizing turbulent behaviour (see [1, 9] for an overview of the applications of contour dynamics). In BSD, however, we discretize the 3D quasi-geostrophic velocity field equations directly without introducing a layered structure in the vertical direction, leading to a remarkably simple numerical algorithm. The assumption of piecewise-constant potential vorticity in the horizontal direction then reduces the 3D model to a 2D problem. An immediate consequence of a direct discretization of the 3D equations is the straightforward treatment of the singularities. In fact, the singular integrals that appear as a result of evaluation of the velocity field at the boundaries of the vortex regions, are easily desingularized by a simple change of variables leading to a robust and stable algorithm. Moreover, since the potential vorticity can be an arbitrary function of the vertical coordinate, variations in the vertical structure of the potential vorticity field are very easily implemented using BSD.

In Sections 2 and 3 we derive equations for the evolution of finite volume vortices in terms of the evolution of the boundary surface enclosing the vortex regions. In Section 4 we discretize the equations and develop the numerical algorithm. In Section 5 we perform basic tests on the algorithm, compare its performance with the well-known exact axisymmetric solution, and present numerical simulations of the

0021-9991/94 $6.00

interaction (merger and combined merger/alignment) of two cylindrical vortices of finite height immersed in a spatially unbounded fluid. Finally a summary and discussion are given in Section 6.

2. PROBLEM FORMULATION

The equation governing large scale motions in an inviscid, rapidly rotating, stratified fluid such as the ocean or atmosphere is the conservation of quasi-geostrophic potential vorticity Q following fluid particles of velocity (u, v) such that

$$\frac{\partial Q}{\partial t}+u\frac{\partial Q}{\partial x}+v\frac{\partial Q}{\partial y}=0, \tag{1a}$$

where

$$Q(x, y, z)=\frac{\partial^2\psi}{\partial x^2}+\frac{\partial^2\psi}{\partial y^2}+\frac{1}{\gamma^2}\frac{\partial^2\psi}{\partial z^2}, \tag{1b}$$

and $\psi(x, y, z, t)$ is the stream function of the horizontal velocity field

$$(u, v)=\left(-\frac{\partial\psi}{\partial y}, \frac{\partial\psi}{\partial x}\right). \tag{2}$$

The variables have been made nondimensional with a characteristic horizontal scale L, a vertical scale D, and a time scale L/U, where U is a characteristic velocity scale. The effect of density stratification is measured by

$$\gamma=L_D/L, \qquad L_D=\mathcal{N}D/f, \qquad \mathcal{N}=\left\{\frac{-g}{\rho}\frac{\partial\rho}{\partial z}\right\}^{1/2}, \tag{3}$$

where L_D is the internal radius of deformation, $\mathcal{N}$ is the Brunt–Väisälä frequency, f is the spatially uniform Coriolis parameter, and $\rho(z)$ is the density. The vertical direction z is parallel to the axis of rotation and the gravitational acceleration $\mathbf{g}$. In obtaining (1b) we made the simplifying assumption that $\mathcal{N}$ is constant which is equivalent to an exponential variation of the density $\rho(z)$.

We note that the vertical component w of the velocity field does not appear explicitly in the equation of conservation of potential vorticity (1a). This expression is valid when the Rossby number $\varepsilon=U/fL\ll 1$ (see, for example, [2, 6]). When a perturbation expansion in ε is used to derive (1), only the $O(\varepsilon)$ term remains in the expansion of w, i.e., $w=w_0+\varepsilon w_1$, with $w_0=0$. Basically this means that to $O(1)$ in ε, fluid particles do not move in the vertical direction. The effect of the $O(\varepsilon)$ term w_1 is implicitly taken into account by the term $\gamma^{-2}\psi_{zz}$ in (1b) which represents vortex stretching in the vertical direction (e.g., see [6] for details).

We now assume a potential vorticity field consisting of three-dimensional regions which are arbitrary functions of the vertical coordinate z, but piecewise-constant in the horizontal x, y-direction. Let V be a finite volume that satisfies these conditions, then

$$Q(x, y, z)=\begin{cases}Q_I(z), & \text{inside } V\\ Q_O(z), & \text{outside } V,\end{cases} \tag{4}$$

where Q_I and Q_O are functions of z only. Once this assumption has been made, (1a) is identically satisfied everywhere except at the boundaries of the vortex region V, where continuity of ψ and its derivatives are satisfied. The two equations (1a), (1b) become decoupled and the problem reduces to the solution of Poisson's equation (1b) on some region $\mathcal{R}$ with appropriate boundary conditions. Let $G(\mathbf{r}, \mathbf{r}')$ be the Green's function of Laplace's operator

$$\frac{\partial^2}{\partial x^2}+\frac{\partial^2}{\partial y^2}+\frac{1}{\gamma^2}\frac{\partial^2}{\partial z^2} \tag{5}$$

satisfying the boundary conditions on $\mathcal{R}$, where $\mathbf{r}=(x, y, z)$, $\mathbf{r}'=(x', y', z')$ are observation and source points, respectively. The solution of (1b) may then be expressed as an integral equation of the form

$$\psi(\mathbf{r}, t)=-\frac{1}{4\pi}\iiint_{\mathcal{R}} Q(\mathbf{r}')\,G(\mathbf{r}, \mathbf{r}')\,dV', \tag{6}$$

where $dV'=dx'\,dy'\,dz'$. Using (2) and (6) the velocity field becomes

$$(u, v)=\frac{1}{4\pi}\iiint_{\mathcal{R}} Q(\mathbf{r}')\left(\frac{\partial}{\partial y}, -\frac{\partial}{\partial x}\right)G(\mathbf{r}, \mathbf{r}')\,dV'. \tag{7}$$

3. SIMPLIFICATION OF THE VELOCITY FIELD EQUATIONS

To simplify the expressions for the velocity field we first note that the Green's function of the operator (5) is symmetric in x, x' and y, y' and hence the x, y-derivatives may be replaced by x', y'-derivatives such that

$$\left(\frac{\partial}{\partial x}, \frac{\partial}{\partial y}\right)G(\mathbf{r}, \mathbf{r}')=\left(-\frac{\partial}{\partial x'}, -\frac{\partial}{\partial y'}\right)G(\mathbf{r}, \mathbf{r}'). \tag{8}$$

Using these relations in (7) we obtain

$$(u, v)=\frac{1}{4\pi}\iiint_{\mathcal{R}} Q(\mathbf{r}')\left(-\frac{\partial}{\partial y'}, \frac{\partial}{\partial x'}\right)G(\mathbf{r}, \mathbf{r}')\,dV'. \tag{9}$$

Next, applying the divergence theorem and a well-known vector identity to the vector fields $\mathbf{i}QG$ and $\mathbf{j}QG$, where $\mathbf{i}$ and

$\mathbf{j}$ are the unit vectors in the x and y directions, respectively, it can be shown that

$$\iiint_{\mathscr{R}} Q(\mathbf{r}')\left(\frac{\partial G}{\partial x'}, \frac{\partial G}{\partial y'}\right) dV' = -\iiint_{\mathscr{R}} G(\mathbf{r}, \mathbf{r}')\left(\frac{\partial Q}{\partial x'}, \frac{\partial Q}{\partial y'}\right) dV'. \tag{10}$$

This is essentially an integration by parts, where the integral over the boundary $\partial\mathscr{R}$ of the region $\mathscr{R}$ can be shown to vanish in the cases of interest to us. Using (10) the velocity field in (9) may be written as

$$(u, v) = \frac{1}{4\pi}\int dz' \iint_{\mathscr{A}} G(\mathbf{r}, \mathbf{r}')\left(\frac{\partial Q}{\partial y'}, -\frac{\partial Q}{\partial x'}\right) dx'\, dy'. \tag{11}$$

We now find the intersection of the volume V with a horizontal plane parallel to the xy-plane at a level $z = z_k$. In other words, we fix a value of z and obtain a two-dimensional plane region bounded by a closed curve $\mathscr{C}$, where the potential vorticity is constant. Hence, applying the same techniques used by Zabusky *et al.* [11] in the development of two-dimensional contour dynamics, the double integrals (11) may be reduced to contour integrals along the closed curve $\mathscr{C}$. The result is

$$(u, v) = -\frac{1}{4\pi}\int_{z_B}^{z_T} dz' \,[Q_O(z') - Q_I(z')] \oint_{\mathscr{C}} G(\mathbf{r}, \mathbf{r}')(dx', dy'), \tag{12}$$

where z_B and z_T are the bottom and top levels of the volume V under consideration. We note that integration of the closed contour from the lower level to the top level of the vortex gives an integral over the closed surface bounding the vortex region V. That is, (12) may now be written in the form

$$(u, v) = -\frac{1}{4\pi}\iint_S \Delta Q(z')\, G(\mathbf{r}, \mathbf{r}')(dx', dy')\, dz', \tag{13}$$

where S is the closed surface enclosing the volume V and

$$\Delta Q(z') = Q_O(z') - Q_I(z') \tag{14}$$

is the potential vorticity difference across the boundary of the vortex region. If there are N_S volumes enclosed by N_S surfaces S_n, $n = 1, \ldots, N_S$, then the velocity field is the sum of the contributions of each volume and

$$u(\mathbf{r}, t) = -\frac{1}{4\pi}\sum_{n=1}^{N_S}\iint_{S_n} \Delta Q_n(z_n')\, G(\mathbf{r}_n, \mathbf{r}_n')\, dx_n'\, dz_n', \tag{15a}$$

$$v(\mathbf{r}, t) = -\frac{1}{4\pi}\sum_{n=1}^{N_S}\iint_{S_n} \Delta Q_n(z_n')\, G(\mathbf{r}_n, \mathbf{r}_n')\, dy_n'\, dz_n'. \tag{15b}$$

Conservation of potential vorticity ensures that fluid particles on the boundary surface S_n remain on the surface. Hence the solution to the problem is now completely determined by evaluation of the velocity field at S_n and using the Lagrangian equations,

$$\frac{dx}{dt} = u(x, y, z, t), \qquad \frac{dy}{dt} = v(x, y, z, t), \tag{16}$$

to calculate the evolution of S_n. The expressions for (u, v) in (15) and the Lagrangian equations (16) constitute the boundary surface dynamics equations describing the nonlinear evolution of continuously stratified geostrophic vortices. The three-dimensional problem (1) has been reduced to the two-dimensional problem of finding the evolution of the self-deforming surfaces enclosing the vortex regions.

It is important to emphasize that since the vertical velocity w does not appear in the potential vorticity conservation (1a), the evolution of the flow is entirely determined by (16), following fluid particles with horizontal velocity (u, v) remaining on the same fixed level z_k throughout the evolution. We also note that the integrals in (15) are surface integrals of a scalar function and therefore the orientation of the surface is not relevant in this case. In principle one may use a suitable parametrization (α, β) and reduce the surface integrals to ordinary double integrals over some region of the (α, β)-plane. This will be used in Section 5 to evaluate the integrals directly at $t = 0$ and provide a basic check on the accuracy and convergence of the numerical algorithm.

4. THE NUMERICAL ALGORITHM

We now write the Green's function in the form

$$G(\mathbf{r}, \mathbf{r}') = G_0(R) + G_1(\mathbf{r}, \mathbf{r}'), \tag{17}$$

where

$$G_0(R) = 1/R, \quad R = [(x - x')^2 + (y - y')^2 + \gamma^2(z - z')^2]^{1/2}, \tag{18}$$

is the singular part of G in the region $\mathscr{R}$ and $G_1(\mathbf{r}, \mathbf{r}')$ is the regular part chosen to satisfy appropriate boundary conditions. Suppose that the boundary surface S (from now on we drop the subscript n for clarity) is discretized by a set of points (x_{ik}, y_{ik}, z_k) such that $0 \leqslant i \leqslant N + 1$ and $1 \leqslant k \leqslant N_z$, where N_z is the number of z-levels and $N + 2$, the number of points on each level. Consequently we obtain the discretized version of (16), viz.,

$$\frac{dx_{ik}}{dt} = u_{ik}, \qquad \frac{dy_{ik}}{dt} = v_{ik}, \tag{19}$$

where $u_{ik} = u(x_{ik}, y_{ik}, z_k, t)$ and $v_{ik} = v(x_{ik}, y_{ik}, z_k, t)$. To simplify the notation we write the velocity field (12) in the form

$$(u, v) = -\frac{1}{4\pi}\int_{z_B}^{z_T} \Delta Q(z')\, M^{(u,v)}(z')\, dz', \tag{20}$$

where

$$M^{(u,v)}(z') = \oint_{\mathcal{C}} [G_0(R) + G_1(\mathbf{r}, \mathbf{r}')](dx', dy'). \tag{21}$$

The superscripts (u, v) refer to the (x', y')-integrals of the (u, v)-components of the velocity field, respectively.

Discretization of the Integrals

We now evaluate (21) at $z' = z_l$ for $1 \leqslant l \leqslant N_z$ and use the convention that $\mathbf{r}_{ik} = (x_{ik}, y_{ik}, z_k)$ denote observation points and $\mathbf{r}_{jl} = (x_{jl}, y_{jl}, z_l)$ denote source points. Then, using a trapezoidal rule gives

$$M^{(u)}(z_l) = \tfrac{1}{2}(x_{1l} - x_{Nl})\, M_{0l} + \tfrac{1}{2}\sum_{j=1}^{N} (x_{j+1\,l} - x_{j-1\,l})\, M_{jl}, \tag{22a}$$

$$M^{(v)}(z_l) = \tfrac{1}{2}(y_{1l} - y_{Nl})\, M_{0l} + \tfrac{1}{2}\sum_{j=1}^{N} (y_{j+1\,l} - y_{j-1\,l})\, M_{jl}, \tag{22b}$$

where

$$M_{jl} = \begin{cases} G_0(R_{jl}) + G_1(\mathbf{r}_{ik}, \mathbf{r}_{jl}), & \text{for } (j, l) \neq (i, k) \\ G_1(\mathbf{r}_{ik}, \mathbf{r}_{jl}), & \text{for } (j, l) = (i, k), \end{cases} \tag{23a}$$

and

$$R_{jl} = [(x_{ik} - x_{jl})^2 + (y_{ik} - y_{jl})^2 + \gamma^2(z_k - z_l)^2]^{1/2}. \tag{23b}$$

To close the contour we have taken $(x_{0k}, y_{0k}) = (x_{N+1k}, y_{N+1k})$ in (22). Finally using the trapezoidal rule in the vertical direction we obtain the velocity field

$$(u_{ik}, v_{ik}) = -\frac{1}{4\pi}\left\{\frac{1}{2}\sum_{l=1}^{N_z-1} (z_{l+1} - z_l)[\Delta Q(z_{l+1})\, M^{(u,v)}(z_{l+1}) + \Delta Q(z_l)\, M^{(u,v)}(z_l)] + I_{ik}^{(u,v)}\right\}. \tag{24}$$

A similar expression may be obtained using Simpson's rule quadrature for more accurate computations. Alternatively, if equally spaced points are not required in the vertical direction, a Gaussian quadrature may be used to give

$$(u_{ik}, v_{ik}) = -\frac{1}{4\pi}\left\{\frac{1}{2}(z_{N_z} - z_1)\sum_{l=1}^{N_z} W_l \times \Delta Q(z_l)\, M^{(u,v)}(z_l) + I_{ik}^{(u,v)}\right\}, \tag{25}$$

where W_l are the weights and z_l are chosen to correspond to the points of the respective Gaussian quadrature for N_z points.

The Singular Integrals

The terms $I_{ik}^{(u)}$ and $I_{ik}^{(v)}$ in (24) and (25) are singular integrals given by the expressions

$$I_{ik}^{(u)} = \int_{z_{k-1}}^{z_{k+1}} \int_{x_{i-1k}}^{x_{i+1k}} \Delta Q(z')\, G_0(R'_{ik})\, dx'\, dz', \tag{26a}$$

and

$$I_{ik}^{(v)} = \int_{z_{k-1}}^{z_{k+1}} \int_{y_{i-1k}}^{y_{i+1k}} \Delta Q(z')\, G_0(R'_{ik})\, dy'\, dz', \tag{26b}$$

where

$$R'_{ik} = [(x_{ik} - x')^2 + (y_{ik} - y')^2 + \gamma^2(z_k - z')^2]^{1/2}. \tag{27}$$

The region of integration is the surface patch containing the singular point $P = (x_{ik}, y_{ik}, z_k)$ shown in the diagram of Fig. 1a. Consistent with the above discretizations, (26) is valid for $i = 0, ..., N$ and $k = 1, ..., N_z$. At the endpoints however, $i - 1$ is replaced by N when $i = 0$ and z_{k-1} and z_{k+1} are replaced by z_1 and z_{N_z} when $k = 1, N_z$, respectively.

To evaluate the integrals, the surface patch is approximated by the section of parabolic cylinder shown in Fig. 1b, using the parametrization

$$\begin{aligned} x' - x_{ik} &= a_1\lambda + b_1\lambda^2, \\ y' - y_{ik} &= a_2\lambda + b_2\lambda^2, \\ z' - z_k &= a_3\mu + b_3\mu^2, \end{aligned} \tag{28a}$$

for $-1 \leqslant \lambda \leqslant 1$ and $-1 \leqslant \mu \leqslant 1$, where

$$\begin{aligned} a_1 &= \tfrac{1}{2}(x_{i+1k} - x_{i-1k}), \\ b_1 &= \tfrac{1}{2}(x_{i+1k} + x_{i-1k} - 2x_{ik}), \\ a_2 &= \tfrac{1}{2}(y_{i+1k} - y_{i-1k}), \\ b_2 &= \tfrac{1}{2}(y_{i+1k} + y_{i-1k} - 2y_{ik}), \\ a_3 &= \tfrac{1}{2}(z_{k+1} - z_{k-1}), \\ b_3 &= \tfrac{1}{2}(z_{k+1} + z_{k-1} - 2z_k). \end{aligned} \tag{28b}$$

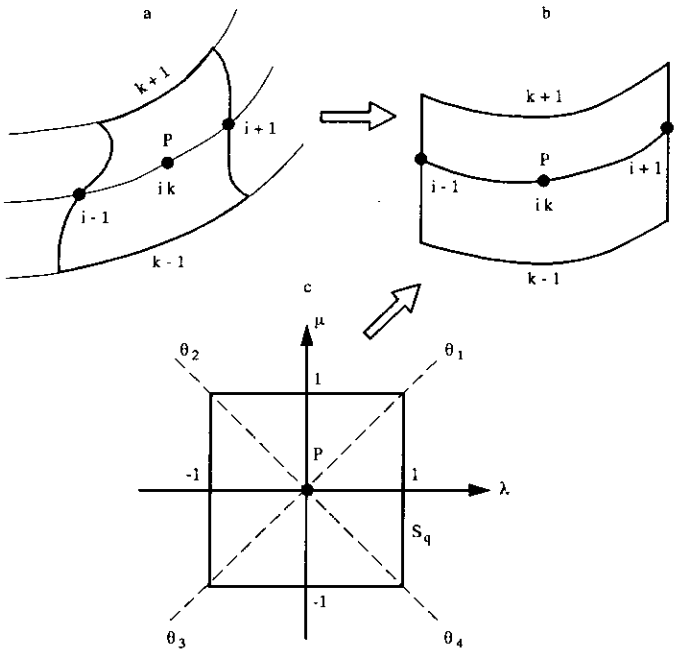

FIG. 1. (a) The surface patch containing the singular point P. (b) Section of parabolic cylinder used to approximate the surface patch. (c) Square region S_q of the λ, μ-plane, where the singular integrals are evaluated.

The integrals over the surface patch become double integrals over the square region of the λ, μ-plane shown in Fig. 1c, and the singular point becomes $(\lambda, \mu) = (0, 0)$. In terms of the new coordinates, (26) may be written in the form

$$I_{ik}^{(u,v)} = \int_{-1}^{1}\int_{-1}^{1} \Delta Q^*(\mu)\, G_0(R_{ik}^*)\, |J^{(u,v)}(\lambda, \mu)|\, d\lambda\, d\mu, \qquad (29a)$$

where the Jacobians of the transformation (28) are

$$J^{(u)}(\lambda, \mu) = \frac{\partial(z', x')}{\partial(\lambda, \mu)}, \qquad J^{(v)}(\lambda, \mu) = \frac{\partial(z', y')}{\partial(\lambda, \mu)}, \qquad (29b)$$

and the asterisks denote the new functions of λ and μ. Finally we transform the double integrals (29) using the plane polar coordinate transformation

$$\lambda = r\cos\theta, \qquad \mu = r\sin\theta, \qquad d\lambda\, d\mu = r\, dr\, d\theta. \qquad (30)$$

Using (27), (28), and (30) we obtain

$$R_{ik}^*(\lambda, \mu) \equiv R_{ik}(r, \theta) = rf(r, \theta), \qquad (31)$$

where

$$f(r, \theta) = [\cos^2\theta(a_1 + b_1 r\cos\theta)^2 + \cos^2\theta(a_2 + b_2 r\cos\theta)^2 + \gamma^2\sin^2\theta(a_3 + b_3 r\sin\theta)^2]^{1/2}.$$

Substitution into (29) and dropping the asterisks gives the non-singular integrals

$$I_{ik}^{(u,v)} = \iint_{S_q} \frac{\Delta Q(r, \theta)}{f(r, \theta)}\, |J^{(u,v)}(r, \theta)|\, dr\, d\theta, \qquad (32)$$

where S_q is the square in Fig. 1c. In practice we divide the square into four triangular regions by the lines $\theta_1 = \pi/4$, $\theta_2 = 3\pi/4$, $\theta_3 = 5\pi/4$, and $\theta_4 = 7\pi/4$ (also shown in Fig. 1c) and compute the resulting integrals using a 6×6 points Gaussian quadrature in each region.

5. NUMERICAL RESULTS

Since the principal aim of this article is to introduce the algorithm and study its feasibility, the numerical simulations are done using the simple case of a spatially unbounded fluid where the Green's function is given in (17) with $G_1 \equiv 0$ and initially take $\gamma = 1$. Consider a circular cylinder vortex of unit radius and unit height such that the bottom and top levels are $z_B = -1$ and $z_T = 0$, respectively. A suitable parametrization is $x' = \cos\alpha$, $y' = \sin\alpha$, and $z' = \beta$, with $0 \leqslant \alpha \leqslant 2\pi$, $-1 \leqslant \beta \leqslant 0$. For the potential vorticity we let $Q_O(z) = 0$, $Q_I(z) = 1$, and hence $\Delta Q(z) = -1$. Using (15) with $N_S = 1$ gives the velocity field

$$(u, v) = -\frac{1}{4\pi}\int_{-1}^{0}\int_{0}^{2\pi} \frac{1}{R}(\sin\alpha, -\cos\alpha)\, d\alpha\, d\beta, \qquad (33)$$

where

$$R = [(x - \cos\alpha)^2 + (y - \sin\alpha)^2 + (z - \beta)^2]^{1/2}.$$

The integrals in (33) were computed directly using a 64×64 ordinary Gaussian quadrature and also a singularity handling routine to at least four decimal places. Table I shows the results at the point $A = (x, y, z) = (1, 0, -1)$. We can anticipate that $u = 0$ at A because any axisymmetric vortex is an exact solution of (1). In particular the cylindrical vortex will rotate without change in shape and constant azimuthal velocity and hence the u-component of the velocity will vanish when $y = 0$.

TABLE I

Direct Computation

	u	v
(a)	0.000000	0.191795
(b)	0.000000	0.191781

(a) Direct computation of (33) at $A = (1, 0, -1)$ using a 64×64 Guassian quadrature. (b) Same as (a) but using a singularity handling routine.

TABLE II

Velocities (u, v) Calculated Using the Algorithm for Trapezoidal and Simpson's Rule Quadratures in the Vertical Direction

		Trapezoidal		Simpson	
N	N_z	u	v	u	v
50	20	0.000853	0.202005	0.000833	0.200621
100	50	0.000175	0.196743	0.000173	0.196536
200	100	0.000043	0.194379	0.000043	0.194303
400	200	0.000010	0.193172	0.000011	0.193141
800	400	0.000003	0.192562	0.000002	0.192549

By comparison Table II gives the (u, v)-components computed at A using the algorithm in Section 4 for trapezoidal and Simpson's rule quadratures in the vertical direction. Although the numbers are approaching the values in Table I, the rate of convergence is slow. This is not surprising since the trapezoidal quadrature (22) is a *second-order* method and we expect the convergence to be $O(1/N)$. Table III shows the convergence for a Gaussian vertical quadrature compared to the corresponding trapezoidal rule for a fixed number of horizontal points ($N = 200$). As expected the Gaussian quadrature performs well even for the small number of vertical levels used in the calculation.

We now investigate the accuracy of the BSD algorithm by studying the evolution of the cylindrical vortex. As mentioned above, the circular cylinder vortex is an exact solution of (1) and hence its original shape will remain unchanged while rotating with constant azimuthal velocity v_0. A standard fourth order Runge–Kutta scheme is used for the time stepping of (16) to $t = 9.6$ with a time step $\Delta t = 0.1$. Figures 2a–c show the relative change in volume

$$\Delta V_o/V_o = [V_o(t) - V_o(0)]/V_o(0),$$

the relative change in the radius at the point A,

$$\Delta r_o/r_o = [r_o(t) - r_o(0)]/r_o(0),$$

TABLE III

Same as Table II, but Comparing Trapezoidal and Gaussian Quadrature in the Vertical Direction

		Trapezoidal		Gaussian	
N	N_z	u	v	u	v
200	12	0.000177	0.199223	0.000115	0.197608
200	16	0.000154	0.197813	0.000081	0.196293
200	20	0.000137	0.197045	0.000059	0.195549
200	24	0.000123	0.196542	0.000044	0.195151
200	32	0.000103	0.195889	0.000027	0.194895

and the relative change in the azimuthal velocity of the point A,

$$\Delta v_o/v_o = [v_o(t) - v_o(0)]/v_o(0),$$

which as mentioned above must all remain constant. Note the decrease in the errors as the resolution is increased for $(N, N_z) = (40, 20)$, $(40, 40)$, $(60, 40)$ (solid, dotted, and dashed lines, respectively). The volume change shows an almost linear increase with time while the change in the radius has an oscillatory behaviour. The azimuthal velocity remains remarkably constant after an initial transient period which itself decreases with increasing resolution.

We now consider the evolution of two identical cylindrical vortices of unit height and initially of unit radius whose centres are separated by a distance $d_c = 2.2$. A Gaussian quadrature is used in the vertical with $N_z = 24$ levels, $N = 70$ horizontal points on each level, and a time step $\Delta t = 0.4$. It can be shown that the volume of each vortex is an invariant of the evolution and this is used to provide a check on the accuracy of the calculations. The relative change in the volumes remained less than 5% in all cases studied here. A typical simulation needed about six hours of CPU time to complete on an Apollo 10000 workstation.

The evolution for $\gamma = 1$ and $\Delta Q = -1$ is shown in Fig. 3. The numbers on the bottom right-hand corner of the boxes indicate the time and those on the top left-hand corner the k-level, i.e., the value of k corresponding to the horizontal cross section $z = z_k$ where the plots were made. Note that, since ΔQ is independent of z in this case, the only z-dependence on the equations comes from (18) and hence the velocity field is symmetric about the middle plane $z = -0.5$. Consequently, only the lower half of the evolution is shown in the figure. The lower end of the structure (levels 1 to 4) evolve in a manner resembling the behaviour of a two-dimensional Eulerian fluid [7, 11], with large filamentary arms being formed. In the middle section (levels 7 to 12), however, the arms begin to disappear and at $t = 21$ this part of the structure has an oval shape with only short thin filaments attached to it. Note also the distortion of the vortex in the vertical direction even for the simple vertical structure $\Delta Q = \text{const}$.

Figure 4 shows the evolution for $\gamma = 0.5$. The initial stages ($t = 7$) are qualitatively similar to Fig. 3. At $t = 21$, however, the filamentary arms of the lower levels become much thinner, although their overall length remains the same. Figure 5 shows the case $\gamma = 0.3$. All levels now look similar to level 12 of Fig. 4 and by $t = 21$ a compact *ellipse-like* structure has formed with only a small amount of filamentation remaining. In fact, decreasing γ even further (not shown here) produced an evolution almost identical to Fig. 5, but where filamentation was completely suppressed. Recalling that small γ implies a horizontal scale large compared to the deformation radius L_D (see (3)), the results are consistent

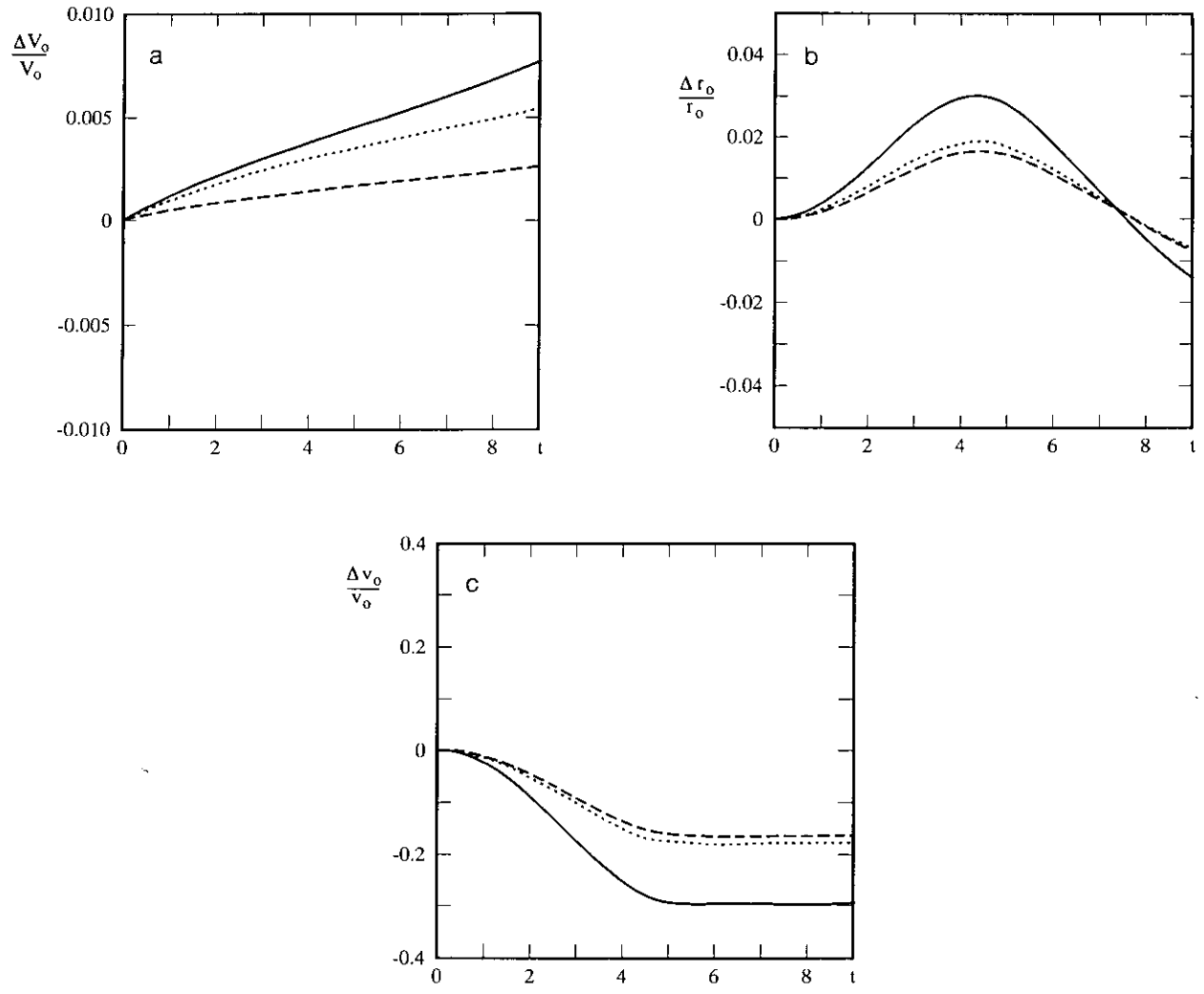

FIG. 2. The relative change of V_0, r_0, and v_0 for $(N, N_z) = (40, 20)$, $(40, 40)$, $(60, 40)$ (solid, dotted, and dashed lines, respectively) as a function of time for $\Delta t = 0.1$. (a) The relative change in volume V_0. (b) The relative change in the radius r_0 at the point A. (c) The relative change in azimuthal velocity v_0 at the point A.

with similar studies of vortex interactions using two-layer quasi-geostrophic models [7, 8].

We now let $\gamma = 4$ and hence the horizontal scale of the flow is less than L_D. The evolution shown in Fig. 6 is qualitatively similar to the Eulerian case on all levels of the vortex. We extended the integration further in time to capture the distortion in the vertical direction which, although less pronounced than before, becomes apparent when comparing levels 1 and 12 at $t = 30$. We emphasize, however, that the similarities with Euler's case are only qualitative in nature. The Green's function is logarithmic in R in that case, compared to the $1/R$ dependence of the Green's function in our model.

So far we have studied the effects of the stratification γ on the pure merger of two vortices at the same level. In the next two examples we fix $\gamma = 1$, move one of the vortices downwards, and consider the possibility of the combined effects of merger and alignment processes working together. The first case is shown in the diagram of Fig. 7a, where the numbers indicate the k-levels plotted in Figs. 7b–c. The lower vortex has its top level $z_T = -0.5$ coinciding with the middle level of the other vortex. Its bottom level is now $z_B = -1.5$. It is convenient to have equally spaced levels and so a Simpson's rule is used in the vertical direction. The results are qualitatively different and more complex than the pure merger cases shown before. This is clearly seen in levels 9 and 17 at $t = 21$, where one of the vortices has become thin and elongated and shows a tendency to engulf the other vortex. The outer levels, in particular 1 and 25, show a clear tendency of vertical alignment as can be seen by the considerable amount of overlap of the two levels.

The final configuration is shown in Fig. 8a, where

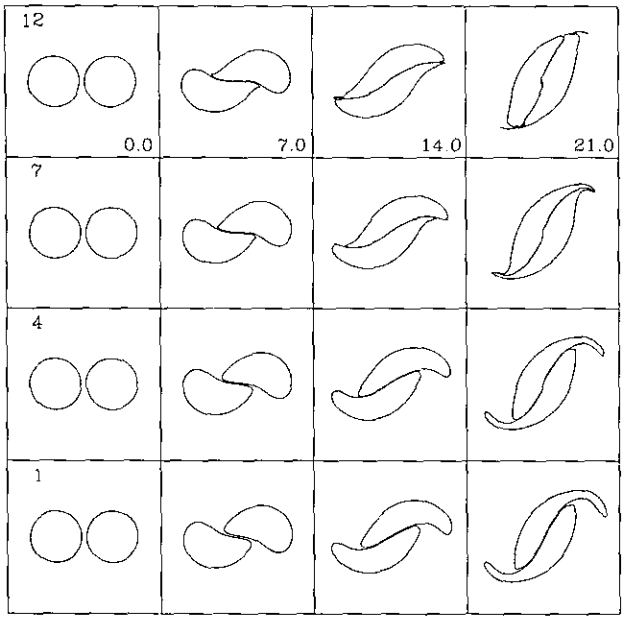

FIG. 3. The evolution for $\gamma = 1$ and $\Delta Q = -1$. Numbers on the top left-hand corner give the level k. Time increases from left to right. $N_z = 24$, $z_1 \equiv z_B = -1$, $z_4 = -0.943$, $z_7 = -0.824$, $z_{12} = -0.532$ (approximately middle level), $z_{24} \equiv z_T = 0$ (not shown).

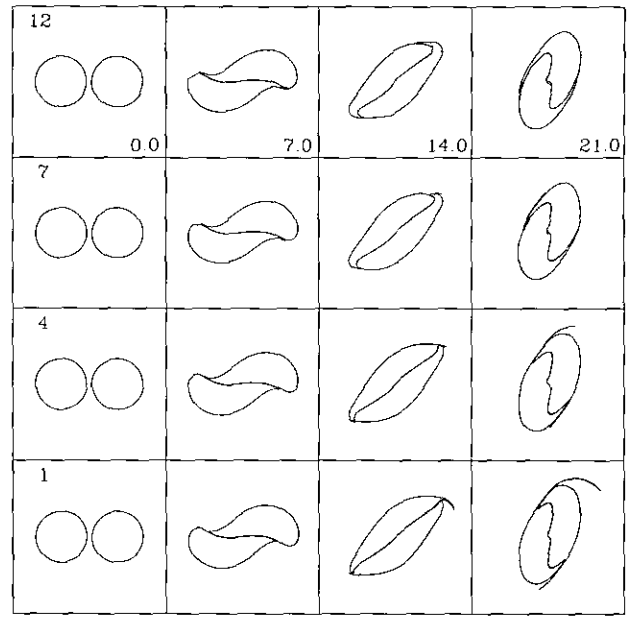

FIG. 5. Evolution for $\gamma = 0.3$.

$z_T = -1$ and $z_B = -2$ on the lower vortex. The evolution of the common level ($k = 17$) is very similar to level 12 of Fig. 7. However, considerable distortion still occurs in the adjacent levels 16 and 19, for example. The outer levels 1, 7 and 25, 33 also show a tendency to overlap at $t = 21$. Extended time integrations will presumably increase the complexity of the structure and the amount of overlap of the outer levels.

6. SUMMARY AND DISCUSSION

We have developed a Lagrangian algorithm for stratified geostrophic vortices consisting of finite volumes of piecewise-constant potential vorticity in the horizontal

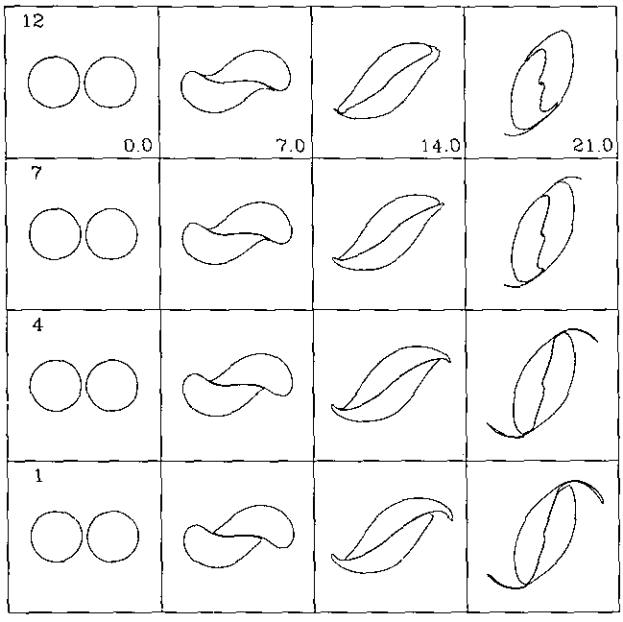

FIG. 4. Evolution for $\gamma = 0.5$. All other parameters as in Fig. 3.

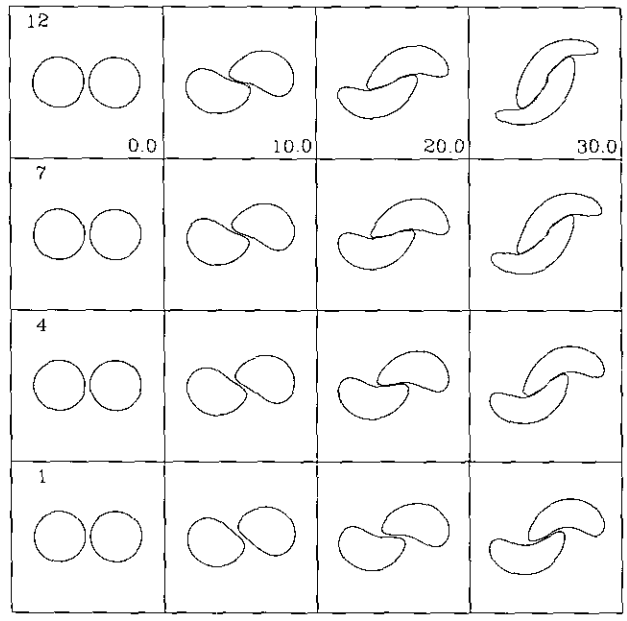

FIG. 6. Evolution for $\gamma = 4$.

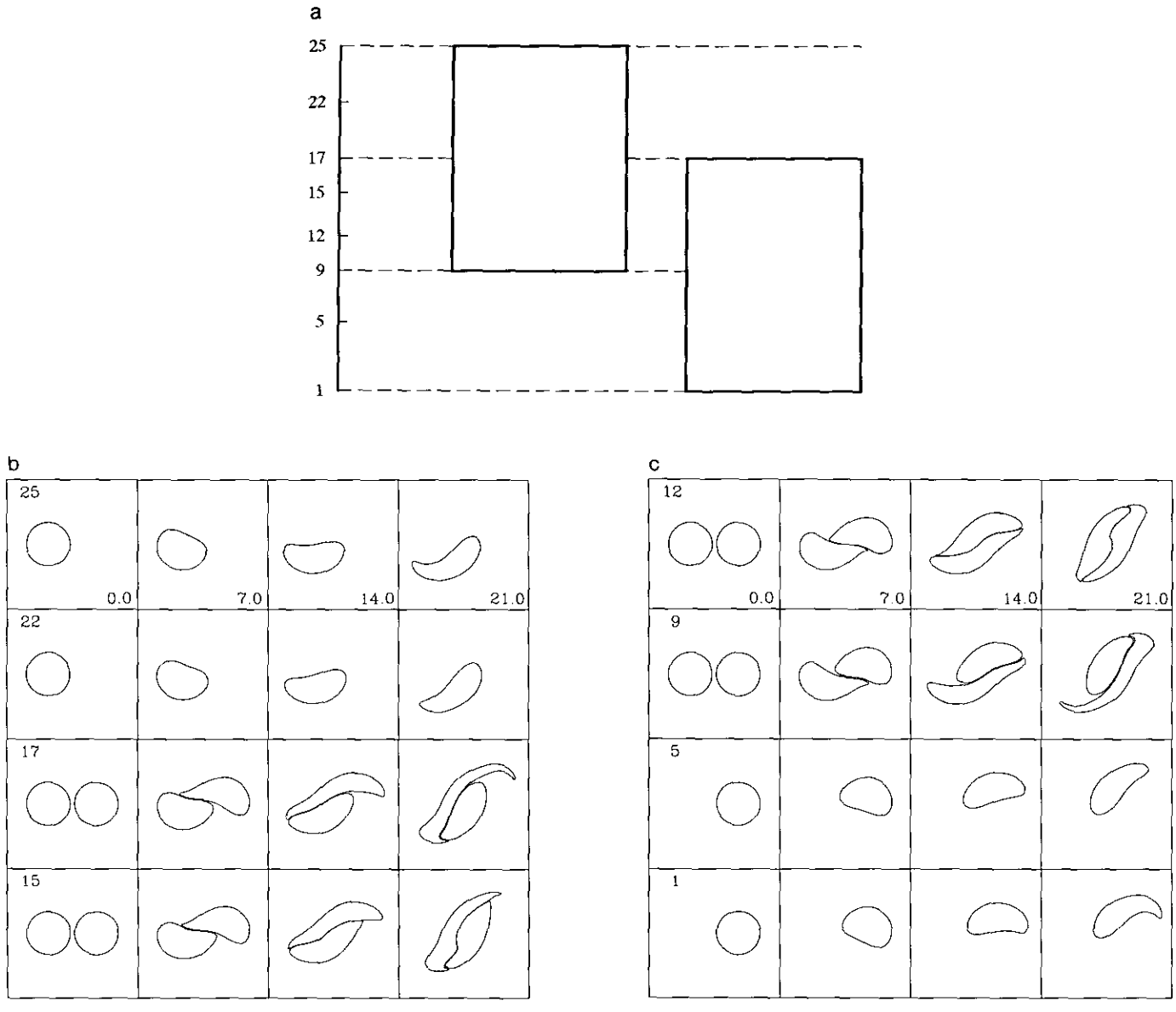

FIG. 7. (a) Side view of the initial position of the vortices. $N_z = 25$, $z_1 = -1.5$, $z_{25} = 0$, $\Delta z = 0.0625$. The numbers indicate the level k; $\gamma = 1$ and $\Delta Q = -1$. (b) The top half of the evolution. (c) The bottom half of the evolution.

direction, in terms of the evolution of the boundary surface enclosing the vortex regions. The potential vorticity, however, may have an arbitrary variation in the vertical direction. Thus, the number of dimensions has been reduced by one, allowing the use of high vertical resolution with greately reduced computational effort. Direct discretization of the 3D velocity field equations results in a simple algorithm without the introduction of a layered structure in the vertical. Moreover, the numerical handling of the singularities is quite straightforward. The simulations showed the effects of varying the stratification γ and the relative vertical positions of two cylindrical vortices. No attempt has been made here to quantify the phenomena caused by continuous stratification or of the many interactions that are possible using this model. However, the results give a preliminary indication of the rich behaviour that might be expected when high vertical resolution of the vortex structure is introduced.

The performance of the BSD algorithm is quite satisfactory when compared with the exact axisymmetric solution as shown in Figs. 2a–c. However, several improvements could be made. For instance, the simple trapezoidal quadrature used in the horizontal direction may be replaced by a higher order interpolation rule such as the cubic scheme

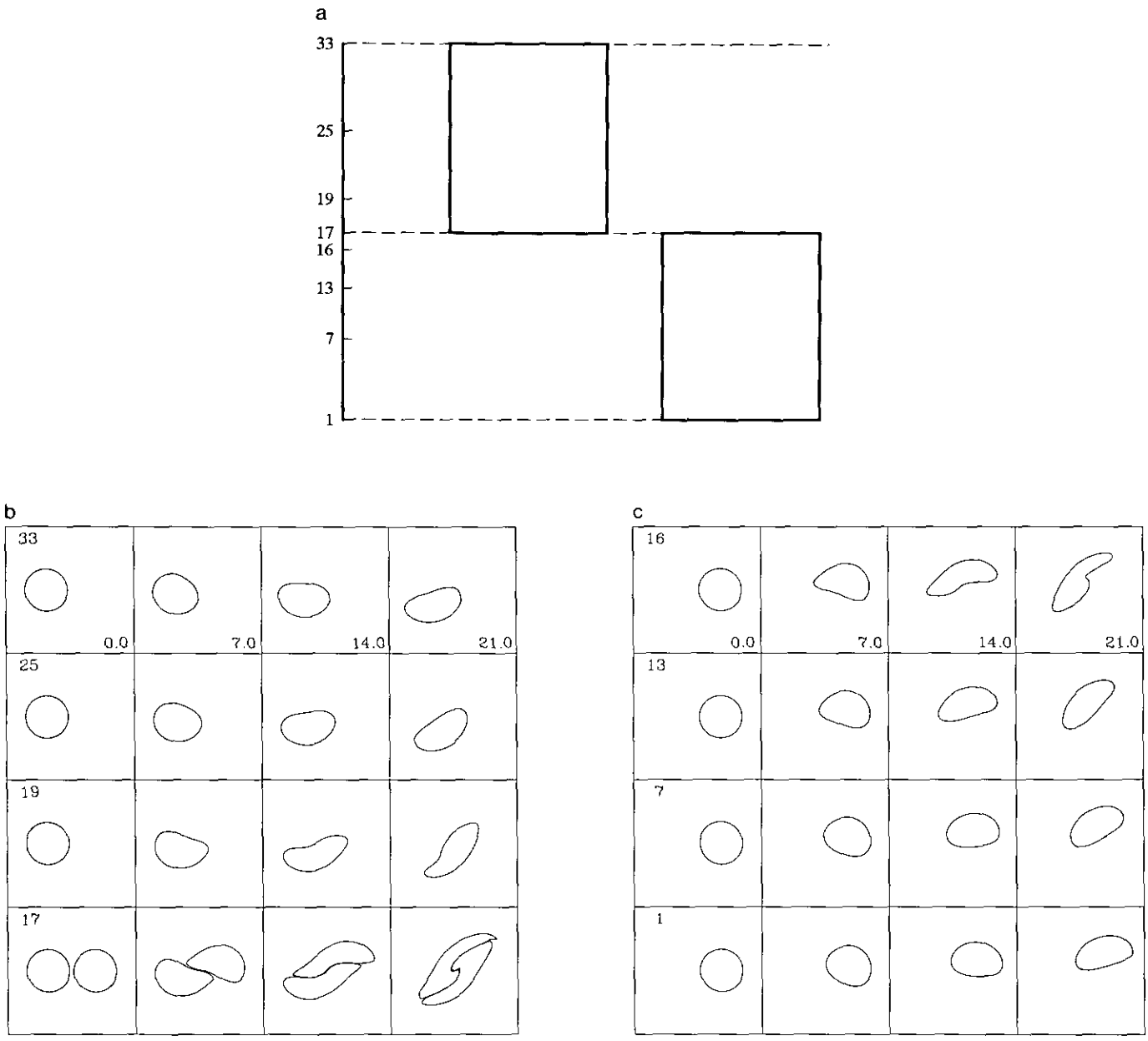

FIG. 8. (a) Side view of the initial position of the vortices. $N_z = 33$, $z_1 = -2$, $z_{33} = 0$, $\Delta z = 0.0625$. Only level 17 is common to both vortices; $\gamma = 1$ and $\Delta Q = -1$. (b) The top half of the evolution. (c) The bottom half of the evolution.

used in contour surgery [1]. The surface patch over which the singular integrals are evaluated may be approximated by a higher order surface patch instead of the simple parabolic cylinder section used in (28). For extended time integrations of high resolution, a node insertion/deletion scheme may be introduced to increase computational efficiency.

A spatially unbounded fluid has been assumed in the simulations in Section 5. However, more realistic boundary conditions can be introduced in the model by choosing the appropriate regular function G_1 in such a way that the Green's function (17) satisfies the specified boundary conditions. Also, in this model we have used a constant density stratification γ. In the case of the oceans and atmosphere, the stratification is not constant but usually varies as a function of the vertical coordinate. When the Brunt–Väisälä frequency is an arbitrary function of z, the potential vorticity is given by $Q = \psi_{xx} + \psi_{yy} + (\gamma^{-2}\psi_z)_z$ (see [6]), of which (1b) is the special case $\gamma = \text{const}$. The

Green's function of this operator also satisfies the symmetry condition (8). Then in principle, the Green's function may be calculated and the same techniques of Section 3 applied to obtain the BSD equations (15) and (16) that are valid for arbitrary stratification.

Finally, it should be pointed out that, although the assumption of piecewise-constant potential vorticity in the horizontal direction appears restrictive, two-dimensional experiments using contour surgery with only eight nested contours to simulate a continuous distribution of vorticity, have shown excellent agreement with pseudo-spectral calculations of similar flows for long-time integrations [1]. It is conceivable that similar agreements may also apply to three-dimensional stratified quasi-geostrophic flows. The comparison of BSD with a pseudo-spectral method will be the subject of future studies.

REFERENCES

1. D. G. Dritschel, *Comput. Phys. Rep.* **10**, 77 (1989).
2. A. E. Gill, *Atmosphere–Ocean Dynamics*, Chap. 12 (Academic Press, New York, 1982).
3. K. R. Helfrich and U. Send, *J. Fluid Mech.* **197**, 331 (1988).
4. B. L. Hua and D. B. Haidvogel, *J. Atmos. Sci.* **43**, 2923 (1986).
5. J. C. McWilliams, *J. Fluid Mech.* **198**, 199 (1989).
6. J. Pedlosky, *Geophysical Fluid Dynamics*, Chap. 6 (Springer-Verlag, Berlin/New York, 1979).
7. L. M. Polvani, N. J. Zabusky, and G. R. Flierl, *J. Fluid Mech.* **205**, 215 (1989).
8. L. M. Polvani, *J. Fluid Mech.* **225**, 241 (1991).
9. D. I. Pullin, *Annu. Rev. Fluid Mech.* **24**, 89 (1992).
10. P. B. Rhines, *Annu. Rev. Fluid Mech.* **11**, 401 (1979).
11. N. J. Zabusky, M. H. Hughes, and K. V. Roberts, *J. Comput. Phys.* **30**, 96 (1979).